

An ultra-flattened chromatic dispersion in circular C₆H₆-infiltrated photonic crystal fibers

Hoang Trong Duc, Nguyen Thi Thuy*



Use your smartphone to scan this QR code and download this article

ABSTRACT

Introduction: In this study, we report a new design of a circular lattice photonic crystal fiber and investigate its optical properties numerically. **Methods:** Near-zero ultra-flattened chromatic dispersion is achieved by allowing benzene (C₆H₆) to infiltrate the hollow core and induce a difference in the air hole size in the cladding. By solving Maxwell's wave equations using the full-vector finite-difference eigenmode, the electromagnetic field modes are analyzed. **Results:** The results show that the variation in dispersion over the broad wavelength range of 527 nm is ± 0.753 ps/nm.km. The nonlinearity coefficient is significantly improved with a value of several thousands W⁻¹.km⁻¹, which is favorable for supercontinuum generation with low input power even though the confinement loss has not yet reached its desired value. **Conclusion:** Two PCFs with optimal lattice parameters and suitable characteristic quantities are selected for supercontinuum generation orientation compatible with application fields such as spectroscopy, temperature sensing, and telecommunication.

Key words: Photonic crystal fiber, ultra-flattened dispersion, C₆H₆ infiltration, high nonlinear coefficient, low confinement loss, Supercontinuum generation

INTRODUCTION

Compared with conventional optical fibers, photonic crystal fibers (PCFs) are preferred in many areas of application due to their special optical properties, such as wideband single-mode operation, high birefringence, great tailorable chromatic dispersion, and higher nonlinearity¹⁻⁶. Ultrashort and intense laser pulses propagating in a nonlinear medium such as PCF lead to the appearance of various nonlinear effects. As a result, the output pulse is continuously broadened. Supercontinuum generation (SCG) performance is strongly influenced by the dispersion profile of the PCF. When the input pulse is pumped in the anomalous dispersion regime, stimulated Raman scattering⁷, including soliton fission (SF) and soliton self-frequency shift (SSFS), is the key nonlinear effect responsible for the quality of the SCG spectrum. However, the presence of solitons causes the spectrum to be noisy. This phenomenon will be eliminated immediately if the PCF is pumped in the normal or all-normal dispersion region. Then, effects such as self-phase modulation (SPM) followed by optical wave breaking (OWB), cross-phase modulation, and four-wave mixing⁸ dominate the spectrum expansion. In this case, the SCG spectrum is smoother, with less noise, but the expansion efficiency is not high.

With design flexibility, PCFs that can achieve flat, near-zero dispersion and higher nonlinearity can satisfy two important elements of SCG quality: spectral width and flatness over broadband wavelengths⁹. Flat, small, and even ultra-flattened dispersion in the broadband wavelength for better SCG has been achieved in PCFs with lattice holes of different sizes, as presented in works¹⁰⁻¹⁶. However, the low nonlinear coefficients and large effective mode area are unfavorable for efficient SCG processes, which are still reported¹²⁻¹⁵. In recent years, liquid core PCFs with highly nonlinear coefficients have become a useful solution that is being widely studied both numerically and experimentally to replace traditional glass core PCFs. Dispersion has been improved markedly, and the quantities characterizing the nonlinear properties of PCF have suitable values, helping to increase SCG efficiency. Diverse dispersion profiles can be easily obtained, including flat all-normal and anomalous dispersions, as expected in liquid-infiltrated PCFs such as toluene^{17,18}, carbon tetrachloride^{19,20}, chloroform²¹, benzene^{22,23}, nitrobenzene^{24,25}, and carbon disulfide^{26,27}. These publications also demonstrate the ability to generate a broader SCG spectrum together with a significant improvement in the peak power of the input pulse. It is even possible to achieve a broad SCG spectrum up to 2900 nm in benzene in-

University of Education, Hue University,
34 Le Loi, Hue City, Vietnam

Correspondence

Nguyen Thi Thuy, University of Education, Hue University, 34 Le Loi, Hue City, Vietnam

Email: ntthuy@hueuni.edu.vn

History

- Received: 2023-04-20
- Accepted: 2023-07-20
- Published: 2023-07-31

DOI :

<https://doi.org/10.32508/stdj.v26i2.4074>



Copyright

© VNUHCM Press. This is an open-access article distributed under the terms of the Creative Commons Attribution 4.0 International license.



Cite this article: Duc HT, Thuy NT. An ultra-flattened chromatic dispersion in circular C₆H₆-infiltrated photonic crystal fibers. *Sci. Tech. Dev. J.* 2023; 26(2):2808-2820.

filtrated PCF^{22,23}. Even so, an ultra-flattened dispersion with low values and near zero has not yet been found in these PCFs. Many researchers have been striving to develop PCFs with ultra-flattened near-zero dispersion to further improve the quality of SCG. By combining the modification of the structural parameters and infiltration of C₆H₆ into the hollow core of the PCF, we designed circular lattice PCFs with different air hole diameters and lattice constants in the cladding. Then, we simulate light propagation in these PCFs to achieve both all-normal and anomalous dispersion configurations. In particular, ultra-flattened and near-zero anomalous dispersion, with a low value of ±0.753 ps/nm km in the wavelength region of 527 nm, was obtained. Furthermore, quantities that characterize nonlinear properties such as nonlinear coefficients, effective mode area, and attenuation also obtain values suitable for SCG applications.

MATERIALS-METHODS

Lumerical Mode Solution (LMS) software was used to model the structure of the PCF circular lattice. First, the Sellmeier coefficient of the refractive index's real parts of SiO₂ is calculated according to Equation (1)²⁸ and declared in the system data. Then, the circular lattice is selected from the available data of symmetric geometries. The core center coordinates, core diameter values D_c, and diameter d of air holes are computed and matched to create a hollow core fiber with 8 rings of parallel air holes along the axis center. Finally, benzene is filled into the hollow core of the PCF by determining and entering the refractive index coefficients from Cauchy's equation (2) of C₆H₆²⁹. The survey wavelength was varied from 0.5 to 2.0 μm.

$$n_{C_6H_6}^2(\lambda) = 2.170184597 + 0.00059399\lambda^2 + \frac{0.02303464}{\lambda^2} + \frac{0.000499485}{\lambda^4} + \frac{0.000178796}{\lambda^6} \tag{1}$$

$$n_{SiO_2}^2(\lambda) = 1 + \frac{0.6694226\lambda^2}{\lambda^2 - 4.4801 \times 10^{-3}} + \frac{0.4245839\lambda^2}{\lambda^2 - 1.3285 \times 10^{-2}} + \frac{0.8716947\lambda^2}{\lambda^2 - 95.341482} \tag{2}$$

Figure 1a shows the cross-sectional geometry of the PCF. The crystal lattice is circular in shape. The cladding has 8 rings of air holes that are evenly spaced parallel to the axis of the hollow core, which is filled with C₆H₆. The design diversity of PCFs with different lattice types or air hole sizes makes it easier to control the dispersion characteristics³⁰. Furthermore, work^{10,31} also demonstrates that the dispersion properties, including the dispersion configuration and wavelength shift at which the dispersion is

zero (ZDW), are strongly dictated by the air hole size in the innermost ring. The other rings are responsible for the loss of PCFs in the basic mode or some cases in higher order. Many results testify that it is not easy to optimize the optical properties of PCF at the same time, so dispersion optimization is still considered the most necessary in SCG research. From these ideas, we designed the diameter (d₁) of the air hole of the innermost ring to be smaller than the others (d₂). The distance from the axis of the PCFs to the air holes in the innermost ring is Λ₁, which is different from the distance between the two adjacent air holes Λ, with Λ₁ = 1.09Λ. The filling factor d₂/Λ was kept constant at 0.95. The lattice constant Λ was chosen as follows: Λ = 0.9 μm, 1.0 μm, 1.5 μm and 2.0 μm. The optical properties of the structures were investigated according to the variation of d₁/Λ, from 0.3 to 0.65 for each 0.05. During the design of PCFs, the core size of the PCFs is also a factor that should be considered. Neither too large nor too small a core size is necessary because the electromagnetic field modes will easily leak into the coating if the core size is too large. In contrast, a core that is too small makes the actual fabrication process more difficult. In our study, the core size is calculated by the formula D_c = 2Λ - 1.2d₁. The cross-section of an optical fiber is divided into hundreds of thousands of small rectangles, known as "Yee meshes"³². A minimum mesh step of 10⁻⁶ μm and 300 mesh cells without override regions are set for the PCFs.

The dispersion and nonlinear properties of the C₆H₆-infiltrated PCFs were simulated by solving Maxwell's wave equation with the full-vector finite-difference eigenmode method (FDE). For accurate simulation, FDE divides the fiber cross-section into hundreds of thousands of very small rectangles with the assumption that the loss of C₆H₆ is negligible. The selected boundary conditions are perfectly matched layers with strong absorption of the waves coming from the calculated region. This helps the LMS to solve the wave equation without any reflection, obtaining the basic-mode field intensity profile with minimal loss and calculating the propagation β with high accuracy. Figure 1b verifies the fine confinement of the electromagnetic field modes in the core of the PCFs.

The linear refractive index (n) of SiO₂ and C₆H₆ decreases with increasing investigated wavelength, as displayed in Figure 1c. Although C₆H₆ has a higher linear refractive index value than SiO₂, the difference is not too large. This makes the process of coupling standard and liquid-core fibers in the fabrication of PCFs more convenient. Furthermore, C₆H₆ has much higher nonlinearity than SiO₂ (n₂ =

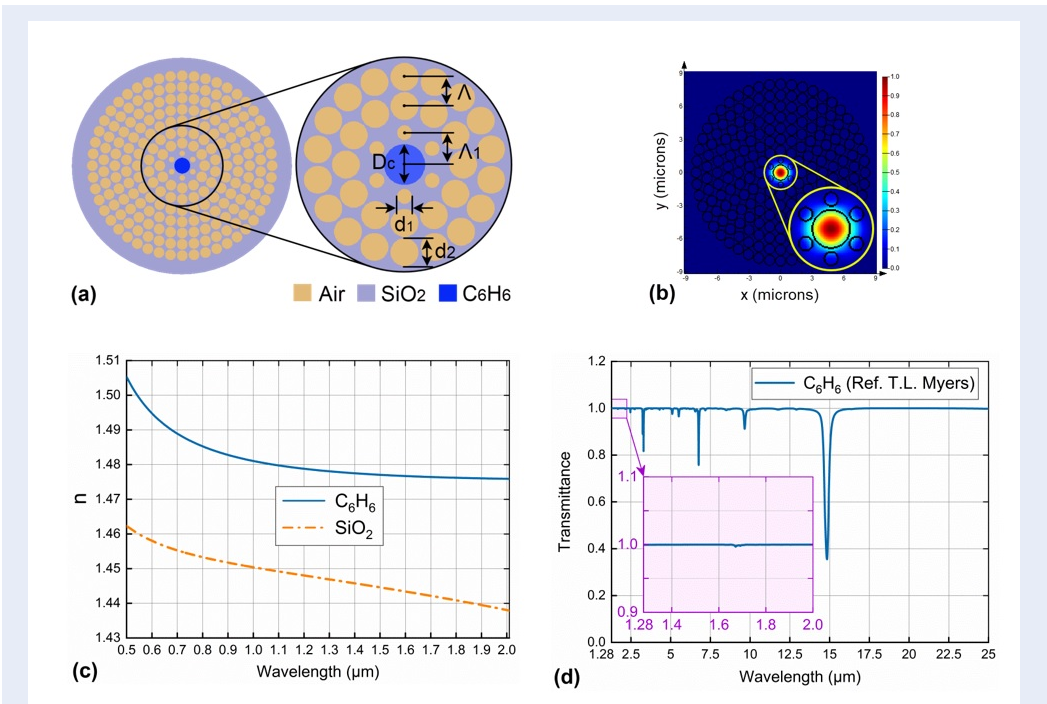


Figure 1: The cross-sectional geometry of PCF with SiO₂ substrate (light-blue): the central hole is infiltrated to benzene (dark blue) and eight parallel rings of air holes (yellow) along the central axis (a); the light confinement in PCF with $\Lambda = 1.0 \mu\text{m}$, $d_1/\Lambda = 0.5$ (b); the real parts of the refractive index n of C₆H₆ and SiO₂ is extrapolated using Sellmeier's and Cauchy's equation (c); and transmission spectrum of C₆H₆ for the temperature of 20 °C is based on experimental data from ³³ (d): the smaller figure (purple) displays the transmittance of C₆H₆ with wavelengths of 1.28 – 2.0 μm .

$169.75 \times 10^{-20} \text{ m}^2 \cdot \text{W}^{-1}$)³³ is approximately 60 times that of SiO₂ ($n_2 = 2.74 \times 10^{-20} \text{ m}^2 \cdot \text{W}^{-1}$)³³. This will result in high nonlinearity of the PCF and improve dispersion, including flatness and value, which is beneficial for SC processes. In addition, the transmittance of C₆H₆ is in a very broad wavelength range from 1.28 μm to 25 μm ³³, and the strongest absorption peak is at approximately 15 μm , with some lower peaks at 2.6 μm , 7.5 μm , and 10 μm . In the investigated wavelength region of 0.5 μm to 2.5 μm (smaller figure), the absorption peaks are very small at approximately 1.67 μm wavelength corresponding to a k value (imaginary part of the refractive index) of 4×10^{-5} . Then, the attenuation A factor is calculated according to the formula³⁴, which has a corresponding value of $23.3 \times 10^{-3} \text{ dB/cm}$. In our numerical model, optical fiber losses are mainly attributed to the material loss of C₆H₆, as shown in Figure 1d, but these fibers have very low losses when $\lambda < 1.67 \mu\text{m}$. When λ is larger, the fiber loss is assumed to be $23.3 \times 10^{-3} \text{ dB/cm}$.

The LMS with the full-vector finite-difference eigenmode (FDE) method has been used to create a C₆H₆-

filled PCF and achieve the field intensity profile of the fundamental mode of the PCF. The data on wavelength-dependent characteristic quantities of all PCFs, including the effective refractive index, dispersion, nonlinear coefficient, effective mode area, and loss, are obtained. Different frequency components of the input pulse propagate at different velocities in nonlinear media, causing dispersion. This dispersion is affected by the size and location of the air holes in the cladding. Thus, achieving preferred values of dispersion, including value, number of ZDWs, and flatness, often depends on the structural design and choice of fiber material. A low dispersion value with a flat profile having one or more ZDWs is the main requirement for achieving coherent SC. Furthermore, the nonlinear effects occurring during the SCG process are related to the occurrence of solitons or non-solitons depending on the all-normal or anomalous dispersion properties of PCFs. The total fiber dispersion includes material dispersion D_m and waveguide dispersion D_w , which is determined by Equation (3)³⁵.

$$D = D_m + D_w = -\frac{\lambda}{c} \frac{d^2 \text{Re} [n_{\text{eff}}(\lambda)]}{d\lambda^2} \quad (3)$$

Here, $\text{Re}[n_{eff}]$ is the real part of n_{eff} , and c is the speed of light in a vacuum.

The nonlinear coefficient is an important parameter that directly affects the spectral extension and input pulse peak power. Normally, PCFs with high nonlinearities are preferred in SCG. In addition, the higher the nonlinearity of the PCF is, the lower the input pulse peak power required for the SCG process. The nonlinear coefficient (γ) characterizes the nonlinearity of the medium, which is determined by Equation (4) below³⁵

$$\gamma(\lambda) = 2\pi \frac{n_2}{\lambda A_{eff}} \quad (4)$$

where n_2 is the nonlinear refractive index of SiO₂ and the effective mode area A_{eff} is inversely proportional to the nonlinear coefficient. The effective mode area is also a vital factor of an optical fiber because it determines how tightly the light is confined to the core and is related to the nonlinear effect in the fiber. A_{eff} is computed through the horizontal electric field across the cross-section of the PCF as Equation (5)³⁵ below:

$$A_{eff} = \frac{(\int_{-\infty}^{\infty} \int_{-\infty}^{\infty} |E|^2 dx dy)^2}{\int_{-\infty}^{\infty} \int_{-\infty}^{\infty} |E|^4 dx dy} \quad (5)$$

where E is the electric field amplitude.

As light propagates in the PCF, the power gradually decreases with the propagation distance and is characterized by the confinement loss L_c . It is calculated through the wavelength and imaginary part of the effective refractive index according to Equation (6)³⁵ below:

$$L_c = 8.686 \frac{2\pi}{\lambda} \text{Im}[n_{eff}(\lambda)] \quad (6)$$

RESULTS

The refractive index difference between the cladding and core is the main cause for the light restriction in the core of PCFs. Therefore, it is necessary to investigate the effective refractive index first and then determine the other characteristic parameters. The propagation constant (β) is related to the effective index of the fiber and can be computed using $\beta = n_{eff}K_0$ ³⁶, with K_0 denoting the free space wavenumber $K_0 = \frac{2\pi}{\lambda}$ ³⁶. The real part of the effective refractive index ($\text{Re}[n_{eff}]$) of the basic mode in the study wavelength region from 0.7 μm to 2.5 μm has been found and quoted in Figure 2. In all cases, the further toward the long wavelength, the more monotonically $\text{Re}[n_{eff}]$ decreases with respect to the structural differences of the PCFs. Again, $\text{Re}[n_{eff}]$ decreases

with increasing filling factor d_1/Λ at a particular wavelength, but it increases with increasing Λ . The interaction between the input pulse and the medium will be stronger if the fiber has a smaller core, resulting in a small $\text{Re}[n_{eff}]$ ³⁷. Therefore, PCFs with smaller lattice constants ($\Lambda = 0.9 \mu\text{m}$; $1.0 \mu\text{m}$) exhibit more pronounced $\text{Re}[n_{eff}]$ changes.

The highest and lowest values of $\text{Re}[n_{eff}]$ at 1.55 μm are calculated and presented in Table 1 they are 1.453 and 1.35, respectively, for PCFs with $\Lambda = 2.0 \mu\text{m}$, $d_1/\Lambda = 0.3$ and $\Lambda = 0.9 \mu\text{m}$, $d_1/\Lambda = 0.65$.

Figure 3 depicts the effect on the chromatic dispersion profile at different lattice constants Λ and filling factors d_1/Λ . The chromatic dispersion characteristics significantly depend upon the air hole diameter of the innermost ring and lattice constant Λ , which form the circular arrangement. Both dispersion curves lying completely below the horizontal axis (all-normal dispersions) and intersecting the horizontal axis at one or two points (anomalous dispersions) are observed. Moreover, the ZDWs move toward the higher frequency range with increasing d_1/Λ when Λ is larger (1.5 μm and 2.0 μm) (Table 2).

When $\Lambda = 0.9 \mu\text{m}$, PCFs with $d_1/\Lambda = 0.3 - 0.45$ have anomalous dispersion with one ZDW. Unlike the large Λ case, the ZDW shifts toward longer wavelengths as d_1/Λ rises. Especially with $d_1/\Lambda = 0.45$, the ZDW has a value of 1.531 μm (Table 2), which helps us to consider the selection of pump wavelengths suitable for commercial laser sources in practice. We obtain four all-normal dispersion profiles with $d_1/\Lambda = 0.5 - 0.65$, where the dispersion curve with $d_1/\Lambda = 0.5$ is flattest and closest to zero. When Λ is increased to 1.0 μm , this dispersion curve shifts very close to zero dispersion, becoming ultra-flattened. The flatness covers a broadband wavelength of 527 nm with a low dispersion value of ± 0.753 ps/nm.km. With ethanol infiltration into the hollow core of SiO₂-based PCFs, work³⁸ achieved a symmetric ultraflat value of 1.04 ps/nm.km normal dispersion in the 500 nm range. An ultra-flattened chromatic dispersion of ± 0.947 ps/nm.km was observed with flatness above 500 nm wavelength in publication¹⁸ when using toluene to fill the hollow core of SiO₂-based PCFs. Thus, it can be seen that the dispersion profile with $\Lambda = 1.0 \mu\text{m}$ and $d_1/\Lambda = 0.5$ has a lower value and the wavelength region has a broader flat dispersion than the works^{18,38}. Compared with the #CBF₁ fiber (circular lattice) in reference²³, the #F₂ fiber in this study also has all-normal dispersion, but it is flatter, and the dispersion value at 1.55 μm is much smaller. This can be beneficial for SC generation with a very broad SC spectrum with nonsoliton dynamics.

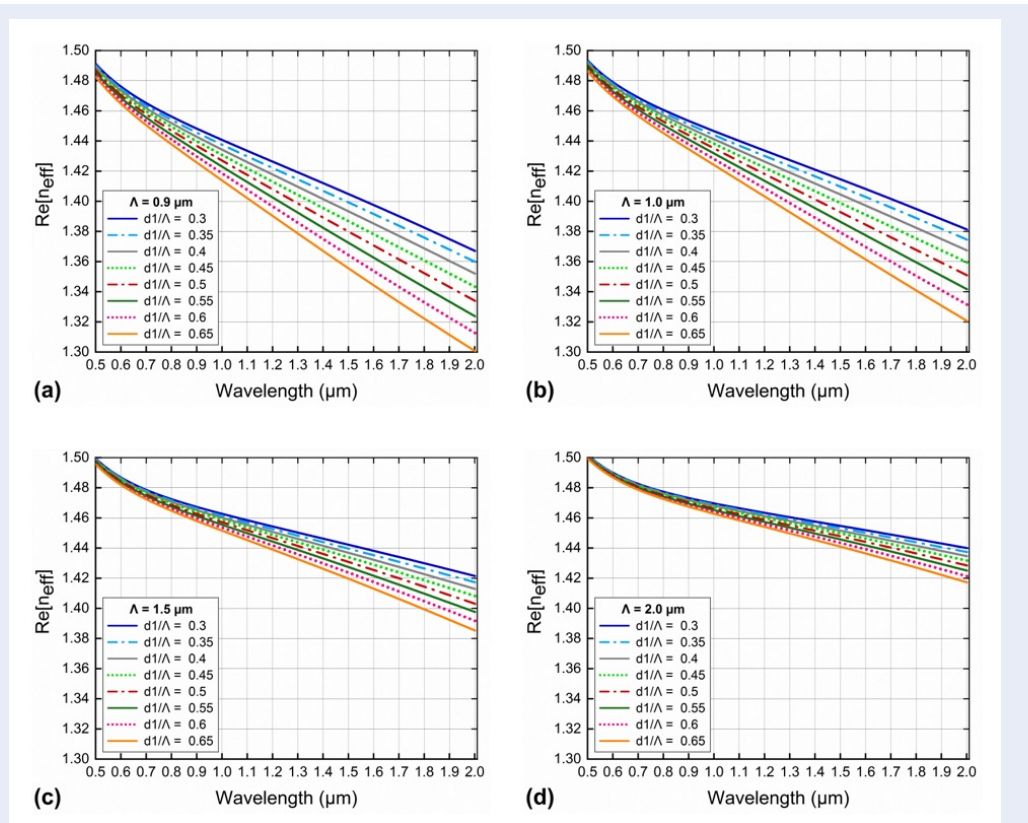


Figure 2: The $Re[n_{eff}]$ as a function of wavelength for different values of d_1/Λ and Λ , with $\Lambda = 0.9 \mu\text{m}$ (a), $1.0 \mu\text{m}$ (b), $1.5 \mu\text{m}$ (c), and $2.0 \mu\text{m}$ (d)

Table 1: $Re[n_{eff}]$ at a $1.55 \mu\text{m}$ wavelength of PCFs with various d_1/Λ and Λ

d_1/Λ	$Re[n_{eff}]$			
	$\Lambda = 0.9 \mu\text{m}$	$\Lambda = 1.0 \mu\text{m}$	$\Lambda = 1.5 \mu\text{m}$	$\Lambda = 2.0 \mu\text{m}$
0.3	1.401	1.411	1.44	1.453
0.35	1.395	1.406	1.438	1.452
0.4	1.389	1.401	1.435	1.45
0.45	1.383	1.395	1.431	1.448
0.5	1.375	1.389	1.428	1.446
0.55	1.368	1.382	1.425	1.444
0.6	1.359	1.375	1.421	1.441
0.65	1.35	1.367	1.416	1.439

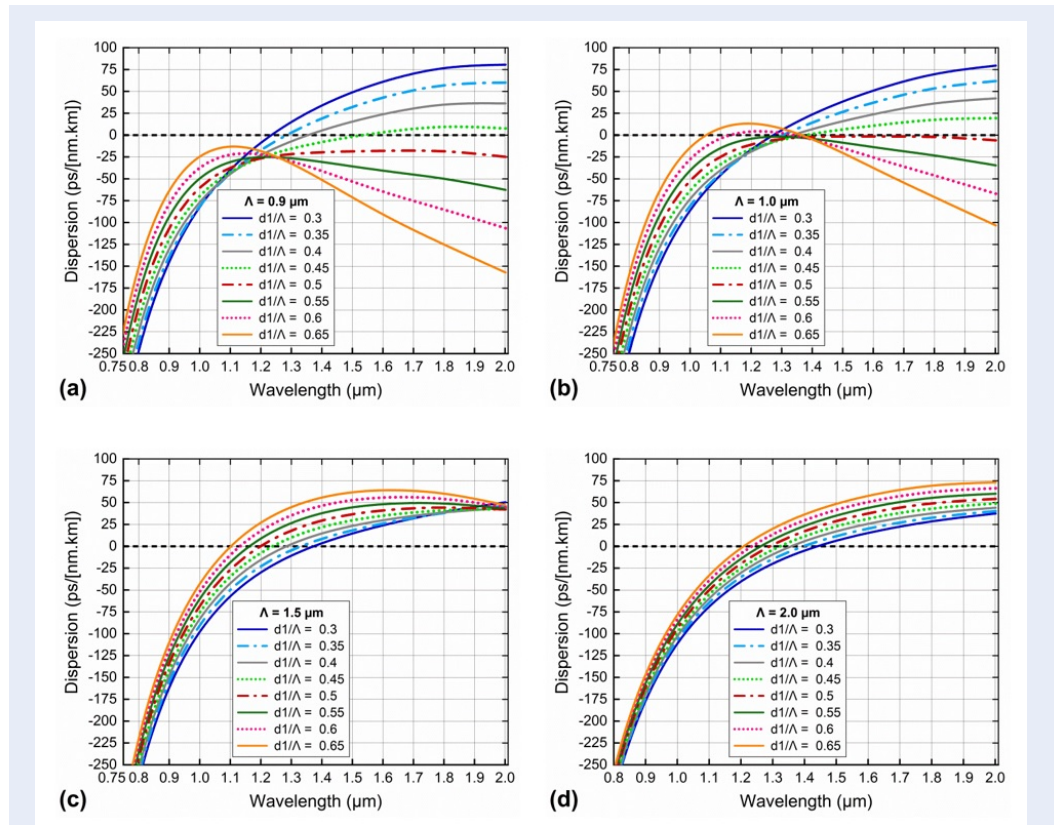


Figure 3: The chromatic dispersion as a function of wavelength for different values of d_1/Λ and Λ , $\Lambda = 0.9 \mu\text{m}$ (a), $1.0 \mu\text{m}$ (b), $1.5 \mu\text{m}$ (c), and $2.0 \mu\text{m}$ (d).

Table 2: The ZDW value of PCFs with various d_1/Λ and Λ

d_1/Λ	$\Lambda = 0.9 \mu\text{m}$		$\Lambda = 1.0 \mu\text{m}$		$\Lambda = 1.5 \mu\text{m}$	$\Lambda = 2.0 \mu\text{m}$
	ZDW _s	ZDW _{s1}	ZDW _{s2}	ZDW _s	ZDW _s	
0.3	1.232	1.272		1.372	1.438	
0.35	1.284	1.302		1.328	1.395	
0.4	1.354	1.334		1.283	1.357	
0.45	1.531	1.377		1.234	1.319	
0.5	D < 0	D < 0		1.198	1.29	
0.55	D < 0	D < 0		1.16	2.001	
0.6	D < 0	1.129	1.342	1.131	1.232	
0.65	D < 0	1.05	1.367	1.1	2.001	

Table 3: Comparison of dispersion values of C₆H₆-infiltrated PCFs with ultra-flattened chromatic dispersion in previous publications

Materials	D (ps/nm.km)	Ultra-flattened dispersion bandwidth (nm)	Refs., Year
Silicate PCF with benzene	±0.753	527	This work
Silicate PCF with toluene	±0.947	500	¹⁸ , 2023
Silicate PCF ₃	±3.345	420	³⁹ , 2021
Silicate PCF ₄	±4.304	492	³⁹ , 2021
Silicate PCF with ethanol	5.0	approximately 500	⁴⁰ , 2020
ZBLAN PCF	1.1	600	⁴¹ , 2019
ZBLAN PCF	1.05	300	⁴² , 2017
Silicate PCF	±0.66	400	⁴³ , 2015

Table 3 compares some PCFs with ultra-flattened chromatic dispersion in previous publications.

For PCFs with larger cores ($\Lambda = 1.5 \mu\text{m}$, $2.0 \mu\text{m}$), the dispersion curves are all anomalous properties with one ZDW. The ZDWs shift toward the short wavelength as d_1/Λ increases. The shift of ZDWs toward short wavelengths can be a disadvantage when suggesting PCFs with suitable pump wavelengths. Normally, the pump wavelengths for SCG are chosen to satisfy two conditions: first, they have a value such that the dispersion is as low as possible; second, they have to match the wavelengths of commercial laser sources in practice. For PCFs with $\Lambda = 2.0 \mu\text{m}$, the anomalous dispersion curve d_1/Λ is closest to zero dispersion, with ZDW having a value of 1.438.

It is not easy to fabricate PCFs with different air hole sizes in the cladding, although this offers great benefits in controlling fiber dispersion and attenuation. PCFs with near-zero ultra-flattened chromatic dispersions have shown the ability to broaden the SCG spectrum with a rather complex structure but can still be fabricated⁴⁰⁻⁴². Furthermore, the publication¹⁸ also reported the ability to achieve near-zero ultra-flattened chromatic dispersion with a small value of ± 0.947 ps/nm.km over a broadband of 500 nm of toluene-infiltrated PCFs, with $\Lambda_1 = 1.095\Lambda$. In this work, to achieve near-zero ultra-flattened chromatic dispersion in PCF infiltrated with C₆H₆, we only changed the lattice parameters of the innermost ring near the core, including the air hole size (d_1) and lattice constant (Λ_1). To clearly see the difference in flatness of dispersion, we compare two dispersion curves with parameters $\Lambda_1 = \Lambda$, $d_1/\Lambda = 0.5$ (green curve) and $\Lambda_1 = 1.09\Lambda$, $d_1/\Lambda = 0.5$ (orange curve) with $\Lambda = 1.0$

μm , illustrated in Figure 4. The green curve is not flat and has a rather high dispersion value. While the orange curve is flatter, ultra-flattened chromatic dispersion covers from 1343 nm to 1870 nm with a dispersion value of ± 0.753 ps/nm.km.

DISCUSSION

In SCG, the various nonlinear effects that govern the characteristics of the spectrum relate mainly to the dispersion profiles of PCFs. To obtain smooth, low noise, flat peaks, and high coherence spectra that result from SPM effects followed by OWB, PCF is used with an all-normal dispersion regime. An ultrabroad SC spectrum in the PCF is generated due to the interaction between several nonlinear effects, including SE, SSFS, and Raman scattering, in the anomalous dispersion region. Although the spectrum achieved is much wider than that of the SCG using PCF with all-normal dispersion, the coherence is lower and the noise is more. This results in a larger input pulse power. However, SCG with different spectral properties in each case has its own application. Therefore, optimization to achieve diverse dispersion profiles is essential. The optimization criteria for generating supercontinuum at the chosen $1.55 \mu\text{m}$ wavelength were flatness, the indication of dispersion properties, and the difference between ZDW and pump wavelength.

Based on the above dispersion analysis, we propose two PCFs with optimal dispersion suitable for SCG to discuss more characteristic quantities, such as dispersion chromatic, nonlinear coefficient, effective mode area, and confinement loss (Figure 4). The first PCF ($\#F_1$) with parameters $\Lambda = 0.9 \mu\text{m}$ and $d_1/\Lambda =$

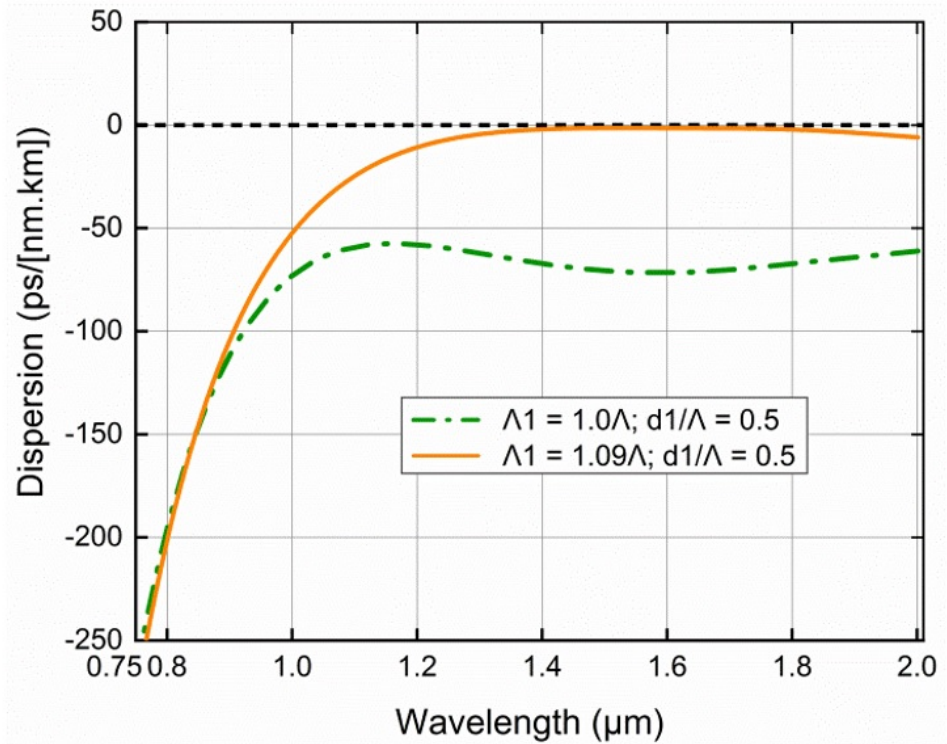


Figure 4: Dispersion characteristic of two PCFs with the difference in the distance from the core to air-holes of the first ring: the green dispersion curve of a PCF with no difference in the distance from the core to the air-holes of the rings ($\Lambda_1 = \Lambda, d_1/\Lambda = 0.5$), the orange dispersion curve of a PCF has differences in the distances from the core to the air hole of the first and other rings ($\Lambda_1 = 1.09\Lambda, d_1/\Lambda = 0.5$), with $\Lambda = 1.0 \mu\text{m}$.

0.45 emits a highly coherent supercontinuum in the anomalous regime at a pump wavelength of $1.55 \mu\text{m}$ (Figure 4a). There are three reasons for this selection. First, this fiber has the flattest anomalous dispersion and the closest to zero among the studied anomalous dispersion curves. Second, it has the ZDW at $1.531 \mu\text{m}$, which is the closest wavelength compared to the one pumped. Third, #F₁ has a low dispersion value of 0.883 ps/nm.km at a $1.55 \mu\text{m}$ pump wavelength. Those are in favor of spectral broadening, effective suppression, and dynamics of noise generation. Second fiber #F₂ ($\Lambda = 1.0 \mu\text{m}, d_1/\Lambda = 0.5$) will produce a very broad SCG spectrum, flat top, higher coherence, and lower noise with low input peak power. This fiber has near-zero ultra-flattened chromatic dispersion spanning a broadband wavelength. There is no ZDW for PCF with all-normal dispersion, so the fiber is pumped at a wavelength close to the local maximum of the dispersion curve. The low dispersion value at a $1.55 \mu\text{m}$ pump wavelength is -1.447 ps/nm.km (Figure 4a).

The nonlinear properties of these two fiber structures are studied in detail. Figure 4 (b, c, d) depicts the dependence of the nonlinear coefficient, effective mode area, and confinement loss on the wavelength. As the wavelength increases, the nonlinear coefficient decreases. At wavelengths greater than $1.67 \mu\text{m}$, the nonlinear coefficients of the two fibers are quite close, but they are separate in the remaining wavelength region. At a $1.55 \mu\text{m}$ pump wavelength, the γ value of the #F₁ fiber is $2726.561 \text{ W}^{-1}.\text{km}^{-1}$, which is higher than that of #F₂ ($2621.599 \text{ W}^{-1}.\text{km}^{-1}$) (Figure 4b). Because of the inverse relationship between the effective mode area and the nonlinear coefficient, the A_{eff} of the #F₁ fiber ($2.531 \mu\text{m}^2$) is smaller than that of the #F₂ fiber ($2.632 \mu\text{m}^2$) (Figure 4c). PCFs with larger core sizes typically exhibit poorer light confinement because light modes easily leak from the core to the cladding or between air holes in the cladding. The confinement loss increases with wavelength and increases rapidly in the long wavelength region ($\lambda > 1.67 \mu\text{m}$), which is consistent with the above analysis of the transmission spectrum of C₆H₆. The L_c values of #F₁

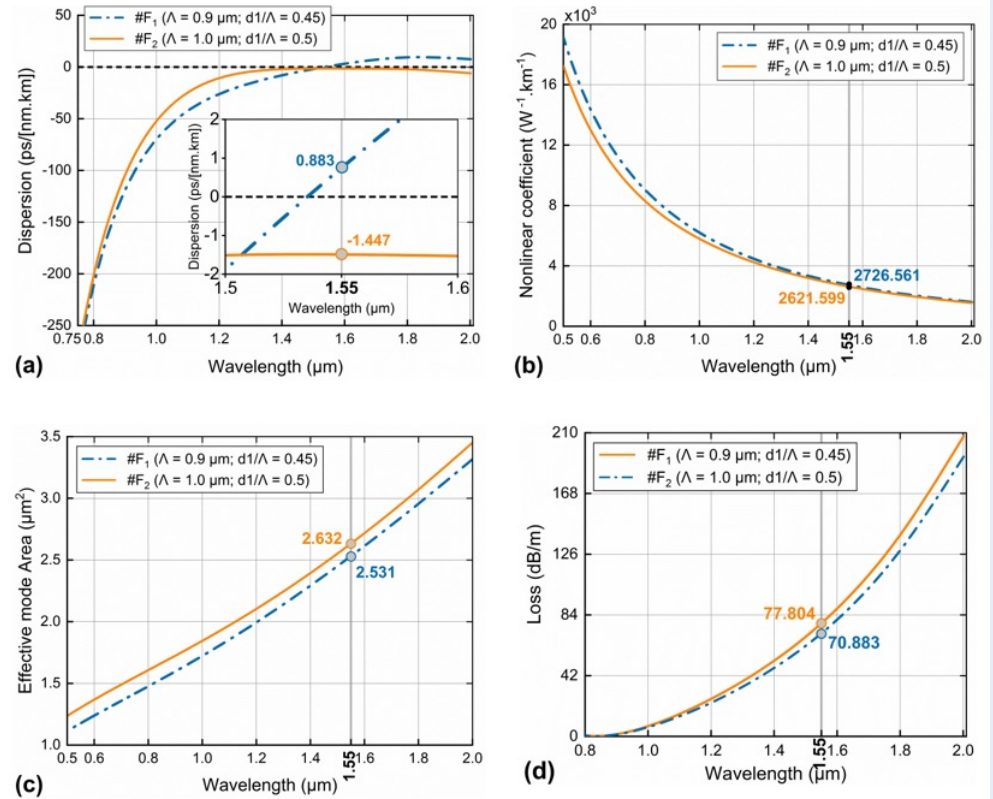


Figure 5: The optical properties of two proposed PCFs: #F₁ (Λ = 0.9 μm, d₁/Λ = 0.45), #F₂ (Λ = 1.0 μm, d₁/Λ = 0.5) (a) the relationship between dispersion and wavelength of #F₁ and #F₂ fibers, the dispersion value at 1.55 μm is 0.883 and -1.447 ps/nm.km, respectively, enlarged in the right inset. (b) the increase of the nonlinear coefficient against the wavelength, values of 2726.561 and 2621.599 W⁻¹.km⁻¹ at the 1.55 μm pump wavelengths of #F₁ and #F₂ fibers. (c) the increase of the wavelength rises the effective mode area with values of 2.632 and 2.531 μm² at the 1.55 μm pump wavelength of #F₁ and #F₂. (d) the confinement loss is proportional to wavelength with value of 77.804 and 70.883 dB/m at the 1.55 μm pump wavelength of #F₁ and #F₂.

and #F₂ at a 1.55 μm pump wavelength are 77.804 and 70.833 dB/m, respectively. The #F₁ fiber has higher loss but lower dispersion and a higher nonlinear coefficient at the pump wavelength, which will improve the SCG efficiency. Table 4 describes the structural parameters at the pump wavelength of the two optimal fibers and compares them with some previous work.

The two optimal PCFs #F₁ and #F₂ have flat dispersion and much lower dispersion values than works^{21,44-46}. In particular, a near-zero ultra-flattened dispersion was not found in these works. With a combination of skillful modification of structural parameters and selection of C₆H₆ to fill the hollow core, the two proposed PCFs have higher nonlinear coefficients than^{21,44,46}, which suggests that when using these PCFs for the SCG process, the peak power may be lower than that of PCFs previously infiltrated

with other fluids. Although the confinement loss of the two proposed PCFs is higher than that of previous publications^{44,46} (Table 4), the flat dispersion and low dispersion value will help the SCG spectrum to be extended. It can be seen that it is very difficult to obtain flat dispersion and low value while simultaneously limiting confinement loss. Depending on the different application purposes of the SCG, a PCF with suitable optical characteristics will be preferred.

CONCLUSIONS

We numerically simulate the chromatic dispersion and nonlinear properties of the C₆H₆-filled PCF by using the FDE. Numerical calculations and simulations reveal that the PCFs exhibit diverse dispersion properties, including all-normal and anomalous dispersion, which strongly depend on the change in lattice constant Λ and the filling factor d₁/Λ. Further-

Table 4: The structure parameters and the characteristic quantities of #F₁ and #F₂ fibers at the pump wavelength in comparison with some other liquid-infiltrated PCFs

#	D _c (μm)	Λ (μm)	d ₁ /Λ	Pump wavelength (μm)	A _{eff} (μm ²)	γ (W ⁻¹ .km ⁻¹)	D (ps/mm.km)	I _c (dB/m)
#F ₁	1.314	0.9	0.45	1.55	2.531	2726.561	0.883	77.804
#F ₂	1.4	1.0	0.5	1.55	2.632	2621.599	-1.447	70.833
#F ₁ ²¹ chloroform	0.643	1.0	0.65	1.03	1.5	1290	-24	-
#F ₂ ²¹ chloroform	1.643	2.0	0.65	1.03	4.48	440	7.6	-
#F ₁ ⁴⁴ carbon tetrachloride	1.125	1.5	0.45	1.35	11.83	-	12	1.85
#F ₂ ⁴⁴ carbon tetrachloride	3.56	4.0	0.8	1.064	10.58	-	-4.37	1.58
#I _{0,3} ⁴⁵ toluene	3.28	2.0	0.3	1.55	7.79	2132.575	-7.784	40
#I _{0,35} ⁴⁵ toluene	2.8	2.0	0.5	1.55	78.9	2890.276	-1.19	120
#F ₁ ⁴⁶ tetrachloroethylene	1.28	1.5	0.4	1.56	433.2	156.9	-15	4.0
#F ₂ ⁴⁶ tetrachloroethylene	3.753	4.0	0.45	1.56	16.67	40.79	3.2	4.2
#F ₃ ⁴⁶ tetrachloroethylene	1.198	1.5	0.55	1.03	359.1	189.3	-4.85	5.3

more, a near-zero ultra-flattened dispersion has been achieved with an all-normal dispersion profile, with dispersion variation as low as ± 0.753 ps/nm.km covering the 527 nm wavelength region. Therefore, it can be used to generate a broadened and smooth supercontinuum spectrum. Two optimal structures, #F₁ and #F₂, with flat dispersion and a high nonlinear coefficient are proposed and analyzed in detail for SCG application orientation. In the case of a C₆H₆-filled core, PCFs can produce a reasonably broad spectrum when injected at 1.55 μ m. The nonlinear coefficients of the two fibers as high as several thousand W⁻¹.km⁻¹ show that liquid-core PCF could be an interesting approach for powerful compact all-fiber systems for SCG with low-power femtosecond pumping systems in the fields of spectroscopy, temperature sensing, and telecommunication, ... There have been many publications on the study of SCG using other liquids-infiltrated PCFs by experiment^{19,44,47}. Therefore, the two optimal structures #F₁ and #F₂ completely meet the requirements of investigating the SCG process both by simulation and experiment. Carbon tetrachloride-infiltrated PCFs with low attenuation^{19,44} are more favorable for broadband SCG all-fiber sources, but the propagation length may be lower than that of toluene-infiltrated fibers⁴⁷. PCFs with benzene can also experience the same phenomenon.

ABBREVIATIONS

SCG: Supercontinuum generation
 PCFs: Photonic crystal fibers
 SPM: Self-phase modulation
 OWB: Optical wave breaking
 SF: Soliton fission
 SSFS: Soliton self-frequency shift
 ZDW: Zero dispersion wavelength
 LMS: Lumerical mode solutions
 FDE: Finite difference eigenmode

COMPETING INTERESTS

The authors declare that they have no conflicts of interest.

AUTHORS' CONTRIBUTIONS

Duc Hoang Trong: designed and simulated the PCF structures, wrote the manuscript, and plotted the graph. Thuy Nguyen Thi: Methodology, Data analysis, Data processing, Manuscript editing, Supervision.

ACKNOWLEDGEMENTS

This research is funded by the University of Education, Hue University, under grant number T.23 – TN – 01.

REFERENCES

- Poudel C, Kaminski CF. Supercontinuum radiation in fluorescence microscopy and biomedical imaging applications. *Journal of the Optical Society of America B*. 2019;36(2):A139-A153; Available from: <https://doi.org/10.1364/JOSAB.36.00A139>.
- Nishizawa N, Kawagoe H, Yamanaka M, Matsushima M, Mori K, Kawabe T. Wavelength dependence of ultrahigh-resolution optical coherence tomography using supercontinuum for biomedical imaging. *IEEE Journal of Selected Topics in Quantum Electronics*. 2019;25(1):1-15; Available from: <https://doi.org/10.1109/JSTQE.2018.2854595>.
- Jahromi KE, Pan Q, Høgstvedt L, Friis SM, Khodabakhsh A, Moselund PM, Harren FJ. Mid-infrared supercontinuum-based upconversion detection for trace gas sensing. *Optics Express*. 2019;27(17):24469-24480; PMID: 31510335. Available from: <https://doi.org/10.1364/OE.27.024469>.
- Yuan J, Kang Z, Li F, Zhang X, Sang X, Wu Q, Yan B, Wang K, Zhou X, Zhong K, Zhou G, Yu C, Lu C, Tam HY, Wai PKA. Mid-infrared octave-spanning supercontinuum and frequency comb generation in a suspended germanium-membrane ridge waveguide. *Journal of Lightwave Technology*. 2017;35(14):2994-3002; Available from: <https://doi.org/10.1109/JLT.2017.2703644>.
- Chen C, Shi W, Reyes R, Yang VX. Buffer-averaging supercontinuum source based spectral domain optical coherence tomography for high speed imaging. *Biomedical Optics Express*. 2018;9(12):6529-6544; PMID: 31065447. Available from: <https://doi.org/10.1364/BOE.9.006529>.
- Smirnov S, Ania-Castanon J, Ellingham T, Kobtsev S, Kukarin S, Turitsyn S. Optical spectral broadening and supercontinuum generation in telecom applications. *Optical Fiber Technology*. 2006;12(2):122-147; Available from: <https://doi.org/10.1016/j.yofte.2005.07.004>.
- Sakr H, Hussein RA, Hameed MFO, Obayya SSA. Analysis of photonic crystal fiber with silicon core for efficient supercontinuum generation. *Optik*. 2019;182:848-857; Available from: <https://doi.org/10.1016/j.ijleo.2019.01.104>.
- Medjouri A, Abed D, Becer Z. Numerical investigation of a broadband coherent supercontinuum generation in Ga₈Sb₃₂S₆₀ chalcogenide photonic crystal fiber with all-normal dispersion. *Opto-Electronics Review*. 2019;27(1):1-9; Available from: <https://doi.org/10.1016/j.opelre.2019.01.003>.
- Dudley JM, Genty G, Coen S. Supercontinuum generation in photonic crystal fiber. *Reviews of modern physics*. 2006;78:135; Available from: <https://doi.org/10.1103/RevModPhys.78.1135>.
- Saitoh K, Koshihara M, Hasegawa T, Sasaoka E. Chromatic dispersion control in photonic crystal fibers: application to ultra-flattened dispersion. *Optics Express*. 2003;11(8):843-852; Available from: <https://doi.org/10.1364/OE.11.000843>.
- Roberts PJ, Mangan BJ, Sabert H, Couny F, Birks TA, Knight JC, Russell PSTJ. Control of dispersion in photonic crystal fiber. *Journal of Optical and Fiber Communications Reports*. 2005;2:435-461; Available from: <https://doi.org/10.1007/s10297-005-0058-9>.
- Medjouri A, Simohamed LM, Ziane O, Boudrioua A, Becer Z. Design of a circular photonic crystal fiber with flattened chromatic dispersion using a defected core and selectively reduced air holes: Application to supercontinuum generation at 1.55 μ m. *Photonics and Nanostructures - Fundamentals and Applications*. 2015;16:43-50; Available from: <https://doi.org/10.1016/j.photonics.2015.08.004>.
- Maji PS, Chaudhuri PR. Supercontinuum generation in ultra-flat near zero dispersion PCF with selective liquid infiltration. *Optik*. 2014;125(20):5986-5992; Available from: <https://doi.org/10.1016/j.ijleo.2014.07.026>.

14. Kumar P, Kumar V, Roy JS. Design of quad core photonic crystal fibers with flattened zero dispersion, AEU - International Journal of Electronics and Communications. 2019;98:265-272; Available from: <https://doi.org/10.1016/j.aeue.2018.11.014>.
15. Hsu JM. Tailoring of nearly zero flattened dispersion photonic crystal fibers. Optics Communications. 2016;361:104-109; Available from: <https://doi.org/10.1016/j.optcom.2015.10.044>.
16. Li XY, Liu P, Xu ZL, Zhang ZY. Design of a pentagonal photonic crystal fiber with high birefringence and large flattened negative dispersion. Applied Optics. 2015;54(24):7350-7357; Available from: <https://doi.org/10.1364/AO.54.007350>.
17. Thuy NT, Duc HT, Bao Tran LT, Trong DV, Lanh CV. Optimization of optical properties of toluene-core photonic crystal fibers with circle lattice for supercontinuum generation. Journal of Optics. 2022;51:678-688; Available from: <https://doi.org/10.1007/s12596-021-00802-y>.
18. Thuy NT, Duc HT, Lanh CV. Supercontinuum generation in ultra-flattened near-zero dispersion PCF with C7H8 infiltration. Optical and Quantum Electronics. 2023;55(1); Available from: <https://doi.org/10.1007/s11082-022-04351-x>.
19. Hoang VT, Kasztelanic R, Filipkowski A, Stępniewski G, Pysz D, Klimczak M, Ertman S, Long VC, Woliński TR, Trippenbach M, Xuan KD, Smietana M, Buczyński R. Supercontinuum generation in an all-normal dispersion large core photonic crystal fiber infiltrated with carbon tetrachloride. Optical Materials Express. 2019;9(5):2264-2278; Available from: <https://doi.org/10.1364/OME.9.002264>.
20. Thuy NT, Duc HT, Bao Tran LT, Lanh CV. Flat-top and broadband supercontinuum generation in CCl4-filled circular photonic crystal fiber. Journal of Nonlinear Optical Physics & Materials. 2022; Available from: <https://doi.org/10.1142/S021886352350042X>.
21. Lanh CV, Van TH, Van CL, Borzycki K, Khoa DX, Vu TQ, Trippenbach M, Buczyński R, Pniewski J. Optimization of optical properties of photonic crystal fibers infiltrated with chloroform for supercontinuum generation. Laser Physics. 2019;29(7):075107-9; Available from: <https://doi.org/10.1088/1555-6611/ab2115>.
22. Lanh CV, Van TH, Van CL, K Borzycki, Khoa DX, Vu TQ, Trippenbach M, Buczyński R, Pniewski J. Supercontinuum generation in benzene-filled hollow-core fibers. Optical Engineering. 2021;60(11):116109; Available from: <http://doi.org/10.1117/1.OE.60.11.116109>.
23. Van LC, et al. Comparison of supercontinuum generation spectral intensity in Benzene-core PCFs with different types of lattices in the claddings. Opt. Quant. Electron. 54, 840 (2022); Available from: <https://doi.org/10.1007/s11082-022-04218-1>.
24. Lanh CV, Van TH, Van CL, Borzycki K, Khoa DX, Vu TQ, Trippenbach M, Buczyński R, Pniewski J. Supercontinuum generation in photonic crystal fibers infiltrated with nitrobenzene. Laser Physics. 2020;30(3):035105; Available from: <https://doi.org/10.1088/1555-6611/ab6f09>.
25. Guo Y, Yuan J-H, Wang K. Generation of Supercontinuum and Frequency Comb in A Nitrobenzene-Core Photonic Crystal Fiber with All-Normal Dispersion Profile. Optics Communications. 2021;481(4): 126555; Available from: <https://doi.org/10.1016/j.optcom.2020.126555>.
26. Lanh CV, Bao Tran LT, Trong DV, Ngoc VTM, Thuy NT, Hong PNT, Minh HTN, Van TH. Supercontinuum generation in highly birefringent fiber infiltrated with carbon disulfide. Optical Fiber Technology. 2023;75:103151; Available from: <https://doi.org/10.1016/j.yofte.2022.103151>.
27. Lanh CV, Khoa DX, Trung LC, Thanh TD, Thuy NT, Hieu VL, Van TH. Supercontinuum generation in chalcogenide photonic crystal fiber infiltrated with liquid. Optical Materials. 2023;137:113547; Available from: <https://doi.org/10.1016/j.optmat.2023.113547>.
28. Tan CZ. Determination of refractive index of silica glass for infrared wavelengths by IR spectroscopy. Journal of Non-Crystalline Solids. 1998;223(1-2):158-163; Available from: [https://doi.org/10.1016/s0022-3093\(97\)00438-9](https://doi.org/10.1016/s0022-3093(97)00438-9).
29. Moutzouris K, Papamichael M, Betsis SC, Stavrakas I, Hloupis G, Triantis D. Refractive, Dispersive and Thermo-Optic Properties of Twelve Organic Solvents in the Visible and Near-Infrared. Applied Physics B. 2014;116(3):617-622; Available from: <https://doi.org/10.1007/s00340-013-5744-3>.
30. Maji PS, Chaudhuri PR. Supercontinuum generation in ultra-flat near zero dispersion PCF with selective liquid infiltration. Optik. 2014;125(20):5986-5992; Available from: <https://doi.org/10.1016/j.ijleo.2014.07.026>.
31. Huang T, Huang P, Cheng Z, Liao J, Wu X, Pan J. Design and analysis of a hexagonal tellurite photonic crystal fiber with broadband ultra-flattened dispersion in mid-IR. Optik. 2018;167:144-149; Available from: <https://doi.org/10.1016/j.ijleo.2018.04.016>.
32. Zhu, Z., Brown, T.G.: Full-vectorial finite-difference analysis of microstructured optical fibers. Opt. Express 10, 853-864 (2002); Available from: <https://doi.org/10.1364/OE.10.000853>.
33. Ho PP, Alfano RR. Optical Kerr effect in liquids. Physical Review A. 1979;20(5):2170-2187; Available from: <https://doi.org/10.1103/PhysRevA.20.2170>.
34. Myers TL, Tonkyn RG, Danby TO, Taubman MS, Bernacki BE, Birnbaum JC, Sharpe SW, Johnson TJ. Accurate measurement of the optical constants n and k for a series of 57 inorganic and organic liquids for optical modeling and detection. Applied Spectroscopy. 2018;72:535-550; Available from: <https://doi.org/10.1177/0003702817742848>.
35. Agrawal G. Chapter 2-pulse propagation in fibers, Nonlinear Fiber Optics (4th edition). Academic Press. 2006:25-50; PMID: 1645588. Available from: <https://doi.org/10.1016/B978-012369516-1/50002-9>.
36. Paul BK, Mactader MdG, Ahmed K, Khalek MdA. Nanoscale GaP strips based photonic crystal fiber with high nonlinearity and high numerical aperture for laser applications. The results in Physics. 2018;10:374-378; Available from: <https://doi.org/10.1016/j.rinp.2018.06.033>.
37. Chen A, Yu Z, Dai B, Li Y. Highly sensitive detection of refractive index and temperature based on liquid-filled D-shape PCF. IEEE Photonics Technology Letters. 2021;33(11):529-532; Available from: <https://doi.org/10.1109/LPT.2021.3073425>.
38. Le HV, Cao VL, Nguyen HT, Nguyen AM, Buczyński R, Kasztelanic R. Application of ethanol infiltration for ultra-flattened normal dispersion in fused silica photonic crystal fibers. Laser Physics. 2018;28:115106; Available from: <https://doi.org/10.1088/1555-6611/aad93a>.
39. Huang Y, Yang H, Zhao S, Mao Y, Chen S. Design of photonic crystal fibers with flat dispersion and three zero dispersion wavelengths for coherent supercontinuum generation in both normal and anomalous regions. The results in Physics. 2021;23:104033; Available from: <https://doi.org/10.1016/j.rinp.2021.104033>.
40. Kumar P, Fiaboe KF, Roy JS. Design of nonlinear photonic crystal fibers with ultra-flattened zero dispersion for supercontinuum generation. ETRI Journal. 2020;42(2):282-291; Available from: <https://doi.org/10.4218/etrij.2019-0024>.
41. Huang T, Wei Q, Wu Z, Wu X, Huang P, Cheng Z, Shum PP. Ultra-flattened normal dispersion fiber for supercontinuum and dissipative soliton resonance generation at 2 μm. IEEE Photonics Journal. 2019;11(3):7101511; Available from: <https://doi.org/10.1109/JPHOT.2019.2915265>.
42. Medjouri A, Meraghni EB, Hathroubi H, Abed D, Simohamed LM, Ziane O. Design of ZBLAN photonic crystal fiber with nearly zero ultra-flattened chromatic dispersion for supercontinuum generation. Optik 2017;135:417-425; Available from: <https://doi.org/10.1016/j.ijleo.2017.01.082>.
43. Medjouri A, Simohamed LM, Ziane O, Boudrioua A, Becer Z. Design of a circular photonic crystal fiber with flattened chromatic dispersion using a defected core and selectively reduced air holes: Application to supercontinuum generation at 1.55 μm. Photonics and Nanostructures - Fundamentals

- and Applications. 2015;16:43-50;Available from: <https://doi.org/10.1016/j.photonics.2015.08.004>.
44. Dinh QH, Pniewski J, Van HL, Ramaniuk A, Long VC, Borzycki K, Xuan KD, Klimczak M, Buczyński R. Optimization of optical properties of photonic crystal fibers infiltrated with carbon tetrachloride for supercontinuum generation with subnanosecond femtosecond pulses. *Applied Optics*. 2018;57(14):3738;Available from: <https://doi.org/10.1364/AO.57.003738>.
 45. Lanh CV, A Anuszkiewicz, A Ramaniuk, R Kasztelan, Khoa XD, M Trippenbach, R Buczynski. Supercontinuum generation in photonic crystal fibers with core filled with toluene. *Journal of Optics*. 2017;19:125604;Available from: <https://doi.org/10.1088/2040-8986/aa96bc>.
 46. Hieu VL, Van TH, Hue TN, Van CL, Buczynski R, Kasztelan R. Supercontinuum generation in photonic crystal fibers infiltrated with tetrachloroethylene. *Optical and Quantum Electronics*. 2021;53:187;Available from: <https://doi.org/10.1007/s11082-021-02820-3>.
 47. Van TH, Rafal K, Alicja A, Grzegorz S, Adam F, Slawomir E, Dariusz P, Tomasz W, Khoa DX, Mariusz K, and Ryszard B. All-normal dispersion supercontinuum generation in photonic crystal fibers with large hollow cores infiltrated with toluene, *Optical Materials Express* Vol. 8, Issue 11, pp. 3568-3582 (2018);Available from: <https://doi.org/10.1364/OME.8.003568>.